

HST Observations of the Gravitationally Lensed Cloverleaf Broad Absorption Line QSO H1413+1143: Modeling the Lens¹

Kyu-Hyun Chae and David A. Turnshek

Department of Physics & Astronomy, University of Pittsburgh, Pittsburgh, PA 15260

ABSTRACT

We investigate gravitational lens models for the quadruply-lensed Cloverleaf BAL QSO H1413+1143 based on the HST WFPC/WFPC2 astrometric and photometric data of the system by Turnshek et al. and the HST NICMOS-2 data by Falco et al. The accurate image positions and the dust-extinction-corrected relative amplifications, along with a possible detection of the lensing galaxy in the infrared, permit more accurate lens models than were previously possible. While more recent models are qualitatively consistent with the HST data, none of the previous models considered the dust-extinction-corrected relative amplifications of the image components. We use the power-law elliptical mass model to fit the HST data. We find that a single elliptical galaxy perturbed by an external shear can fit the image positions within the observational uncertainties; however, the predicted relative magnifications are only roughly consistent with the observational relative amplifications. We find that a primary galaxy combined with a secondary galaxy in the vicinity of the Cloverleaf or a cluster centered (south-)west of the Cloverleaf can fit both the image positions and relative amplifications within the observational uncertainties. We discuss future observations which could be used to test and/or further constrain lens models of the Cloverleaf.

Subject headings: gravitational lensing — quasars: individual (H1413+1143, Cloverleaf)

1. Introduction

The gravitationally-lensed “Cloverleaf” consists of four bright image components of a distant Broad Absorption Line (BAL) QSO H1413+1143 ($z \approx 2.55$; $V \approx 16.8$), which was discovered by Hazard et al. (1984) and later identified to be a lens system by Magain et al. (1988). Since its discovery the search for the lens in optical wavebands has not resulted in a detection (e.g.

¹Based on observations with the NASA/ESA *Hubble Space Telescope*, obtained at the Space Telescope Science Institute, which is operated by AURA, Inc., under NASA contract NAS 5-26555.

Turnshek et al. 1997; hereafter T97) until just recently (Falco et al. 1998). A recent analysis of the Falco et al. HST NICMOS-2 data has shown some evidence for the lensing galaxy near the geometrical center of the Cloverleaf (Kneib, Alloin, & Pelló 1998b), although a spectroscopic identification of the claimed galaxy, along with the measurement of its redshift, could not be done because its faintness and the brightness of the QSO image components preclude this. The observed absorption systems along the line of sight at $z_{abs} \approx 0.61, 1.35, 1.44, 1.66, 1.87, 2.07$ and 2.1 (Monier, Turnshek, & Lupie 1998) have raised the suspicion that the lens might be associated with one or more of the known absorption systems.

The first study of gravitational lens models for the Cloverleaf was based on ground-based optical and VLA observations by Kayser et al. (1990), who found that a singular isothermal elliptical galaxy model and a two-isothermal-spherical-galaxies model could fit their optical image positions and some features of the radio data. However, neither of the Kayser et al. (1990) models was consistent with the observed optical image intensity ratios. In addition, the two-spherical-galaxies model predicted an unobserved “bright” fifth image. Kayser et al. (1990) considered the possibility of microlensing to explain the discrepancy between the model magnification ratios and the observed intensity ratios; either components A & D or B & C should be microlensed according to their models. There have been some observational indications for microlensing of component D in the Cloverleaf (see below and §3). Photometric variations of component D relative to the other components were reported in several observations (Kayser et al. 1990; Remy et al. 1996; Østensen et al. 1997), although T97 did not detect any significant variations between five different HST observing epochs covering 2.76 years. Except for component D, however, there are no observational indications for microlensing in the Cloverleaf (see also Østensen et al. 1997).

More recent modeling attempts for the Cloverleaf were based on HST archival data (optical image positions and intensity ratios) along with CO(7-6) emission data (Yun et al. 1997; Kneib et al. 1998a). Those authors used lens models to study the CO emitting region around the central engine of the QSO. One aspect of particular interest which is common to the lens models of Yun et al. (1997) and Kneib et al. (1998a) is that neither model is a single potential model. For example, the model of Kneib et al. (1998a) considers a possible contribution from a yet-to-be-confirmed distant cluster along with a primary lensing galaxy. These models suggest that the lens in the Cloverleaf is a complicated lens rather than an isolated single galaxy. Keeton, Kochanek, & Seljak (1997; hereafter KKS) argue that many lenses, including the Cloverleaf, can be well-fitted using *two independent shears*, which is also consistent with this point of view.

In this paper we use the HST WFPC/WFPC2 astrometric and photometric data given by T97 to constrain Cloverleaf lens models. In particular, we use the dust-extinction-corrected relative amplifications as lensing constraints. We will also use the position of the putative lensing galaxy given by Kneib et al. (1998b) as a constraint. We will use the generalized power-law mass model described in Chae, Khersonsky, & Turnshek (1998; hereafter CKT) to model the lens. In §2 we briefly review the elliptical mass model of CKT and define the goodness of fit, χ^2 , of a model

to the data. In §3 we investigate gravitational lens models for the Cloverleaf. We first find that a single galaxy model is inconsistent with the T97 data. We then consider lens models consisting of an elliptical galaxy and an external shear. We also consider lens models consisting of two elliptical masses (a primary galaxy + a secondary galaxy; a galaxy + a cluster) in order to fit successfully the dust-extinction-corrected relative amplifications. In §4 we discuss future observations which can test and/or further constrain lens models of the Cloverleaf.

2. Power-Law Elliptical Mass Model

The projected view of a power-law triaxial ellipsoid on the sky (i.e. the lens/image plane) can be represented by the following 2-dimensional elliptical distribution of mass (CKT; see also Keeton & Kochanek 1997)

$$\Sigma(r, \theta) = \Sigma_0 \left\{ 1 + \left(\frac{r}{r_c} \right)^2 [1 + e \cos 2(\theta - \theta_0)] \right\}^{-(\nu-1)/2}, \quad (1)$$

where (r, θ) are the polar coordinates of the lens plane. The power-law elliptical mass (EM; eq. [1]) is described by the following five independent parameters: (1) Σ_0 , the surface density at the center, (2) ν , the radial index such that the deprojected 3-dimensional mass density $\rho \sim r^{-\nu}$ and the isothermal-like distribution is for $\nu = 2$, (3) r_c , the core radius, (4) e , an ellipticity parameter which is related to the true ellipticity, ϵ ($= 1 - q$ where q is the axis ratio) via $\epsilon = 1 - [(1 - |e|)/(1 + |e|)]^{1/2}$, and (5) θ_0 , an orientation angle which is the position angle (P.A., north through east) if $e > 0$.

To fit the observed positions and relative amplifications of the image components (T97) and the observed positions of the lensing galaxy (Kneib et al. 1998b) we define the goodness of fit, χ^2 , as follows

$$\chi^2 = \sum_i \left(\frac{x_{iA}^{th} - x_{iA}^{ob}}{\sigma_{x_{iA}}} \right)^2 + \sum_i \left(\frac{y_{iA}^{th} - y_{iA}^{ob}}{\sigma_{y_{iA}}} \right)^2 + \sum_j \left(\frac{R_{jC}^{th} - R_{jC}^{ob}}{\sigma_{R_{jC}}} \right)^2, \quad (2)$$

where $i = B, C, D, G1$ ($G1$ denoting the primary galaxy) and $j = A, B, D$. The parameters x_{iA}^{th} and x_{iA}^{ob} are the theoretical and observational relative horizontal positions (i.e. right ascensions), respectively, of components $B, C, D, G1$ with respect to component A . The parameters y_{iA}^{th} and y_{iA}^{ob} are the theoretical and observational relative vertical positions (i.e. declinations), respectively, of components $B, C, D, G1$ with respect to component A . The parameters R_{jC}^{th} and R_{jC}^{ob} are the theoretical and observational relative magnifications, respectively, of components A, B, D with respect to component C . Finally, $\sigma_{x_{iA}}$ and $\sigma_{y_{iA}}$ are the observational uncertainties in the relative positions, while $\sigma_{R_{jC}}$ are the observational uncertainties of the relative magnifications. The parameter χ^2 (eq. [2]) is a function of the lens parameters. Given the positions and relative amplifications of the image components and the positions of the primary galaxy along with their

observational uncertainties, the parameters of a lens model are adjusted to minimize χ^2 . For the minimization of χ^2 , we use the so-called downhill simplex method (see Press et al. 1992).

3. Gravitational Lens Models of the Cloverleaf

The HST optical images of the Cloverleaf (T97) provide more accurate and tighter constraints on lens models of the Cloverleaf than any earlier observations. Except for the declination of component D, the relative image positions are measured with an accuracy $\approx 3 - 4$ mas. Table 1 summarizes the T97 astrometric data. These image positions will be used as the primary constraints on the lens models of the Cloverleaf in this study. The photometric data of T97 from the ultraviolet to the near infrared revealed sight-line-dependent dust extinctions for the individual image components. T97 considered two dust models, galactic-like and SMC-like, at two assumed redshifts, $z = 2.55$ and 1.55 . The derived relative amplifications are summarized in Table 2. Among the four dust-extinction models, Model C (galactic extinction at $z = 1.55$) is significantly different from the other models which are similar to one another. The NICMOS-2/F160W intensity ratios (Kneib et al. 1998b) now appear to be inconsistent with Model C (so this model will no longer be considered). The main difference between the derived relative amplifications and the observed intensity ratios in a given filter is that components A and B have significantly larger amplifications after corrections for the dust extinctions. We will use the dust-extinction-corrected relative amplifications as lens model constraints in this study. In previous studies HST optical intensity ratios were used (Yun et al. 1997; Keeton et al. 1997; Kneib et al. 1998a). We will also use the position of the lensing galaxy reported in Kneib et al. (1998b) as a constraint.² This new constraint is important only for a two-galaxy model (§3.3) because a single galaxy model with and without a perturbation field requires the galaxy to be positioned near the geometrical center of the Cloverleaf.

However, one caution should be taken in using the relative amplifications of T97 as lensing constraints, namely any possible contribution from microlensing. As well as the observations of photometric variation of component D mentioned in §1, spectroscopic properties in the Cloverleaf could be interpreted as an evidence of microlensing of component D. In fact, Angonin et al. (1990) favored the interpretation that two spectral features of component D, which were substantially different from the same features in the other components, were the result of microlensing: (1) component D has significantly lower broad emission line (BEL) to continuum flux ratio than the other components and (2) at some outflow velocities the BAL profiles of component D are deeper than the BAL profiles in the other components. The lower BEL/continuum ratio of

²The detected light could be a fifth image rather than a galaxy. This possibility cannot be excluded, especially since a spectroscopic identification of the light has not yet been done. In this paper, however, we will not explore the possibility of a fifth image.

component D than the other components ($A : B : C : D = 0.97 \pm 0.03 : 0.95 \pm 0.03 : 1.00 : 0.70 \pm 0.02$) could be easily explained by microlensing. Namely, the more centrally-concentrated continuum-emitting region is amplified (microlensed) more than the BEL region as seen in component D, thereby lowering its BEL/continuum ratio. In line with this interpretation, several microlensing calculations have been done with assumed models of the BAL clouds to reproduce the distinctive BAL profiles of component D (Hutsemékers 1993; Hutsemékers, Surdej, & Van Drom 1994; Lewis & Belle 1997). Given this microlensing interpretation of component D, the macrolensing relative amplification of component D can be derived by multiplying its observational relative amplification (after correction for dust extinction) by 0.7. Unless specified otherwise, a χ^2 of a model in this paper is given for the amplification Model B with the microlensing interpretation of component D, i.e., the observational relative amplifications used are $R_{AC} = 1.68(0.168)$, $R_{BC} = 1.61(0.161)$, and $R_{DC} = 0.665(0.095)$, where the values in parentheses are the uncertainties we chose.

Another possibility we can envisage for the explanation of the lower BEL/continuum ratio in component D is that the macrolensing magnification ratio of the BEL/continuum is smaller for component D than for the other components. In this case, there is no need for microlensing in component D, and the dust-extinction-corrected relative amplifications will represent the macrolensing magnification ratios. This interpretation could be interesting because the characteristic radius of the BEL region could then be estimated from a study of the functional relationship between the magnification and radius of the extended region. This would, of course, require that the lens model for the Cloverleaf be well constrained. Another observational constraint from the T97 observations is that any unresolved image near the geometrical center of the Cloverleaf should be fainter than $\approx 2.5\%$ of the brightness of component C.³ Finally, we will exclude models which predict very large total magnifications (i.e. larger than ≈ 600) by requiring the QSO to be intrinsically brighter than $M_V \approx -23$, consistent with the spectrum exhibiting BALs.

We calculate the lensing in a standard cosmology with the following values for the cosmological parameters: the deceleration parameter $q_0 = \frac{1}{2}$, the Hubble constant $H_0 = 75h_{75}^{-1} \text{ km s}^{-1} \text{ Mpc}^{-1}$, and the cosmological constant $\Lambda = 0$.

3.1. *Single Galaxy Lens Models: Isolated*

Kayser et al. (1990) considered a singular isothermal elliptical galaxy model for the Cloverleaf. This model corresponds to the special case of $r_c \rightarrow 0$ and $\nu = 2$ in the power-law EM model

³If any dust is present along the line of sight of a fifth image and thus obscures it, this limit should be corrected. In this study, we will ignore such a correction.

described in §2. The singular isothermal model predicted magnification ratios of $A : B : C : D = 0.58 : 1.00 : 1.00 : 0.35$ when constrained with optical image positions available at that time. These ratios are obviously inconsistent with T97’s relative amplifications. Our mass model allows us to consider other values of ν and r_c . The effect of varying r_c is related to the brightness of a fifth image. For a given value of ν , the upper limit on r_c is set by requiring that any fifth image be fainter than 2.5% of the brightness of component C. The low value of 2.5% for the brightness limit of any fifth image means that the upper limit on the core radius is small. For example, the upper limit on the core radius of a model with $\nu = 1.19$ is only $r_c \approx 0.12h_{75}^{-1}$ kpc. Since the image is formed far outside the core radius (at $r \approx 3.5h_{75}^{-1}$ kpc), varying core radius has little effect on the lensing properties of the model. On the other hand, the model is very sensitive to the value of the radial index ν . Shallower mass profiles (i.e. smaller ν) require less elliptical (i.e. more circular) distributions. Mass distributions of different ellipticities predict different relative magnifications, time delays, and total magnifications. Since the isothermal model is inconsistent with the observationally-derived relative amplifications, one is led to vary the radial index from the isothermal value $\nu = 2$. Using the observational constraints of T97, the goodness of fit χ^2 decreases from ≈ 216 to the minimum value of $\chi_{min}^2 \approx 168$ as the value of ν decreases from the isothermal value of 2. The minimum χ^2 is obtained when $\nu = 1.19$. For this model the predicted relative magnifications are $A : B : C : D = 1.15 : 1.16 : 1.00 : 0.85$ (see Table 3). This is much more consistent with the observed relative amplifications when compared to the predictions of the isothermal model. However, it still significantly deviates from the observationally-derived relative amplifications by T97. Moreover, although the main difficulty with the single-galaxy model is the mismatch between the predicted and observed relative amplifications, it cannot reproduce the HST image positions at an acceptable level. Also, even with less sensitive observational constraints than the T97 constraints, KKS obtained $\chi^2 = 148.9$ and 142.0 with a single ellipticity and a single external shear, respectively. Therefore, we conclude that a power-law mass distribution with elliptical symmetry is inconsistent with the observed properties of the Cloverleaf.

3.2. *Single Galaxy Lens Models: With External Tidal Perturbation*

In §3.1 we saw that a single EM lens is inconsistent with the observational constraints. Here we consider the possibility that an external tidal perturbation is present, in addition to a single primary lensing galaxy, and that it significantly contributes to the lensing effect.⁴ The tidal perturbation could be due to a galaxy cluster, of which the lensing galaxy is a member, or a group of galaxies along the line of sight. We use an external shear term to describe the tidal

⁴Calculations similar to that presented here can also be found in KKS, who calculated lens models for several lenses, including the Cloverleaf. However, our calculation for the Cloverleaf is based on the new lensing constraints of T97.

perturbation. The scaled deflection angle of the external shear term is given by Kovner (1987) as

$$\vec{\alpha}_t(\vec{x}) = \gamma \begin{pmatrix} \cos 2\theta_\gamma & \sin 2\theta_\gamma \\ \sin 2\theta_\gamma & -\cos 2\theta_\gamma \end{pmatrix} \cdot \vec{x}, \quad (3)$$

where γ and θ_γ are the shear strength and angle, respectively, and \vec{x} is the scaled position vector on the lens plane (see, e.g., CKT). In order not to increase the number of degrees of freedom of the model compared with the single EM model, we fix the radial index at $\nu = 2$ and the core radius at $r_c = 0.001h_{75}^{-1}$ kpc (even if we allowed the parameters ν and r_c to vary, we would not improve the fit).

This model of an elliptical mass along with an external shear (to be denoted “EM+ γ ” model) can be made to fit the image positions within measurement uncertainties. However, the model cannot be used to obtain a good fit to the relative amplifications. The model has $\chi^2 \approx 12.8$. The fitted model parameters and model predictions can be found in Table 3. Note that the model predictions of R_{BC} and R_{DC} do not match well the observationally-derived relative amplifications. The galaxy has a P.A. of $\approx 140^\circ$, so it is oriented roughly along BC. The shear angle is $\theta_\gamma \approx 44^\circ$, which puts its orientation roughly along AD (orthogonal to the galaxy). If the galaxy is forced to be oriented along AD, then the fitted shear angle tends to be aligned with the galaxy, and the fit becomes much worse. Such a model becomes qualitatively similar to the single EM model considered in §3.1. Thus, in using EM+ γ model to fit the Cloverleaf, it is critical for the galaxy to be oriented along BC. In previous studies, Yun et al. (1997) and KKS also found that an elliptical potential and an elliptical mass, respectively, would be oriented roughly along BC, while a shear would be oriented roughly along AD, consistent with our result. The model predictions of Yun et al. (1997) do, however, differ somewhat from our model predictions; their model predicts $\mathcal{M}_{tot} = 220$ and maximum time delay $\tau_{DC} = 1.9h_{75}^{-1}$ days. The fitted parameters of the KKS model and our model are similar, and the quantitative difference between the two results comes from the fact that we use the dust-extinction-corrected relative amplifications by T97 as constraints. We note that a shear of $\gamma \approx 0.22$ required in the EM+ γ model is somewhat large, and such a strong shear implies an important secondary lensing contributor (see KKS).

3.3. Two-Galaxy Lens Models

In §3.2, we saw that an EM+ γ model does not fit well the observationally-derived relative amplifications (in particular R_{BC}). Here we consider the possibility of the presence of a secondary galaxy near the line of sight, either at the same redshift or at a different redshift from the primary galaxy. The redshift(s) of the lensing object(s) is(are) unknown in the Cloverleaf. We consider the case that two galaxies are at the same redshift and arbitrarily set $z = 1.55$. A lens model consisting of two elliptical masses (to be denoted “EM2” model) has twice as many free parameters as a single-galaxy lens model considered in §3.1. When we describe each galaxy by an EM model,

it is characterized by five parameters (see §2). In addition to the ten parameters of two galaxies, there are four more free parameters in the EM2 model, i.e., the relative position of a galaxy with respect to the other on the lens plane and the two coordinates of the QSO on the source plane.

From now on we will assume that the two galaxies have the same radial index and core radius. Furthermore, we fix the core radius at $r_c = 0.001h_{75}^{-1}$ kpc and the radial index at $\nu = 2$, which is the isothermal distribution. In the two-galaxy model a fifth image can be formed between the two galaxies, and the relative brightness of the fifth image depends on the core radius of the galaxy closest to the fifth image and the mass ratio between the two galaxies. Given the constraint that any fifth image should be fainter than 2.5% of the brightness of component C (T97), it would be reasonable to fix the core radius at a small value. There is no *a priori* reason that the two galaxies should have the same radial index. We have chosen to simplify our analysis by assuming so. With the above assumptions (simplifications) the parameters of the two-galaxy model are (1) the combined central density, Σ_0^{tot} ($= \Sigma_0^{(1)} + \Sigma_0^{(2)}$), (2) the mass fraction of G2, f_2 ($= \Sigma_0^{(2)}/\Sigma_0^{tot}$), (3) and (4) the ellipticities of the two galaxies, ϵ_1 and ϵ_2 , (5) and (6) the position angles of the two galaxies, P.A.₁ and P.A.₂, (7) and (8) the magnitude (d_{12}) and position angle (P.A.₁₂) of the displacement of G2 from G1 (\vec{d}_{12}), and (9) and (10) the two coordinates of the QSO on the source plane. In the above, G1 is the primary galaxy closest to the geometrical center of the Cloverleaf, while G2 is the secondary galaxy.

3.3.1. Secondary Galaxy at an Arbitrary Position

We first consider the possibility of the presence of an undetected secondary galaxy in the vicinity of the Cloverleaf. We find that the two-galaxy model with G2 at an arbitrary position can fit both the QSO image positions and relative amplifications nearly perfectly. However, the position of the primary galaxy is not fitted as well. The value of χ^2 (ranging $\approx 5.4 - 7.7$) is dominated by the mismatch between the model (primary) galaxy position and the observational galaxy position obtained by Kneib et al. (1998b). In fact, if we were not using the galaxy position as a constraint, we would have a perfect fit. The secondary galaxy can be positioned (1) southeast of the primary galaxy within the Einstein ring [Model 1, Table 4; Fig. 1 (a)], (2) north of component D [Model 2, Table 4; Fig. 1 (b)], or (3) southwest of the primary galaxy outside the Einstein ring [Model 3, Table 4; Fig. 1 (c)]. In all of the above cases the secondary galaxy is significantly less massive than the primary galaxy (f_2 ranges from 0.17 – 0.26) so that the secondary galaxy could be even fainter than the primary galaxy which has not been detected at optical wavelengths. The projected separation (d_{12}) between the two galaxies is not uniquely determined, and varying its value does not lead either to a significant change in χ^2 or to different lensing predictions (e.g. time delays, total magnification). Thus, for each model we fixed the parameter d_{12} at an (arbitrarily) chosen value. As Figure 1 (a) shows, in Model 1 an extended region can form a weak fifth image near the center of G2. However, its relative magnification (with

respect to component C) is only $\approx 9 \times 10^{-4}$. In the above two-galaxy lens models the primary galaxy is oriented roughly along AD. As we will see, the two-galaxy model with an arbitrary position for G2 matches the T97 observational constraints better than any of the other models considered in this paper. This is, of course, the result of taking advantage of the freedom in G2's position. As seen above, G2's position cannot be uniquely determined using lensing constraints. However, there are only three regions of sky [see Figure 1 (a), (b), and (c)] in the vicinity of the Cloverleaf which should be considered candidates for where a faint galaxy could be found. Next we consider the two-galaxy model with G2's position constrained.

3.3.2. Secondary Galaxy at the Position of a Detected Object

We examine the possibility that the secondary galaxy is one of the detected objects in the surrounding of the Cloverleaf (see Kneib et al. 1998a,b). Specifically, we consider their object number 14, which is $\approx 4''.5$ north-northeast of component A. From the NICMOS-2 data we derive ($1''.87$, $4''.14$) as the position of the object relative to component A with an error of $0''.07$. However, the object is not bright enough to derive its light distribution. Even if it were possible to derive the light distribution, we could not use it as the mass distribution since the distribution of dark mass, which is likely to account for most of the total mass in the scale of $4''.5$ ($\approx 26h_{75}^{-1}$ kpc), could be significantly different from the light distribution. Thus, we allow the ellipticity and position angle of G2 to be free parameters. This model can fit well both the image positions and relative amplifications, except for R_{DC} . The predicted R_{DC} ($0.31 - 0.56$) is significantly lower than the observational $R_{DC} = 0.67$, which was derived using the microlensing interpretation of the *continuum* of component D from the dust-extinction-corrected relative amplification. However, if the BELR is also microlensed in component D, the macrolensing R_{DC} should be lower than 0.67 and its value would depend on the microlensing amplification factor. Since the microlensing amplification depends on the size scale of the source region, it will be different for the continuum region and the BELR; the smaller continuum region will be more amplified than the more extended BELR. In this case, the discrepancy of R_{DC} can be clearly resolved. For this possibility, in this section (and only in this section) we do not use R_{DC} as a constraint. Instead, we will derive the required microlensing amplification factors for the continuum *and* the BELR using the model.

In the model G2 has to be highly elliptical and the best fitting model is obtained when G2's ellipticity is $\epsilon_2 = 0.84$ [Model 4, Table 4; Fig. 1 (d)]. As ϵ_2 decreases from this value, χ^2 increases rapidly. For a 99% confidence limit $\epsilon_2 \gtrsim 0.58$. As ϵ_2 increases from the best fitting value, χ^2 increases only moderately. The largest ellipticity we consider is $\epsilon_2 = 0.94$. The predicted R_{DC} and required microlensing amplification factors of the continuum and BELR are shown in Figure 2 as a function of ϵ_2 within the 99% confidence limit. In the model the primary galaxy has a relatively small ellipticity and is oriented roughly along BC, as opposed to the other two-galaxy models considered in §3.3.1.

Although the model considered in this section is a good candidate for the correct lens model of the Cloverleaf, it is still possible that the BELR is extended enough so that it is unaffected microlensing. In this case the discrepancy of R_{DC} should be explained in other ways (e.g. G2 may be at a different redshift from G1), or the model should be discarded. The model could also be discarded if it could be determined that G2 is less massive and/or less elliptical than required in the model [in the model the total mass of G2 within $4''.5$ is $\approx (0.66 - 3.3) \times 10^{12} M_{\odot}$ for $0.58 \lesssim \epsilon_2 \lesssim 0.94$]. At present we do not know if the model is the true description of the lens. This is a posteriori reason that we explore other models (§3.3.1 and §3.4).

3.4. *Galaxy+Cluster Lens Models: A Model-Dependent Bound on the Mass of the Lensing Galaxy*

In this section we re-examine the possibility that a cluster is present and makes a significant contribution to the lensing. Although an external shear term considered in §3.2 could qualitatively account for the lensing contribution of the cluster, the ignored higher-order terms (rather than the quadrupole term) may be important. In this case one must model the cluster, for example, using an elliptical mass distribution. Since the properties of the possible cluster are unknown at present, we make several assumptions about the mass distribution of the cluster for studying its lensing effect. We consider an isothermal mass distribution ($\nu = 2$) for the cluster and fix the core radius at $r_c = 40h_{75}^{-1}$ kpc. The chosen core radius is similar to the value of $33h_{75}^{-1}$ kpc used by Kneib et al. (1998a). It is also in the same order of magnitude as the isothermal core of $23h_{75}^{-1}$ kpc for the cluster 0957+561 as determined from weak lensing effect by Fischer et al. (1997). We fix the ellipticity of the cluster at $\epsilon = 0.5$. Buote & Canizares (1996) derive $\epsilon_{mass} \approx 0.40 - 0.55$ for isothermal mass models using ROSAT observations of five Abell clusters and assuming hydrostatic equilibrium. De Theije, Katgert, & van Kampen (1995) find that the ellipticity peaks at $\epsilon \sim 0.4$ and extends to $\epsilon \sim 0.8$ from an analysis of a large set of 99 low-redshift Abell clusters. In the above, however, the exact values of r_c and ϵ are less important for our purpose since the lensing effect is not very sensitive to these parameters. Kneib et al. (1998a) found that an overdensity of objects around the Cloverleaf could be centered $\approx 7''.8$ southwest of component A. Consistent with their finding, we fix the separation between the galaxy mass center and the cluster mass center at $d_{12} = 8''$. However, we allow the position angle of the cluster from the galaxy, P.A.₁₂, to be a free parameter. The exact value of d_{12} is less important since varying d_{12} does not lead either to a significantly-improved fit or to different lensing predictions. On the other hand, varying the parameter P.A.₁₂ can lead to a significant change in χ^2 and also to different lensing predictions. The parameter P.A.₁₂ can be varied by varying the parameter f_2 , since the fitted value of P.A.₁₂ is determined by the chosen value of f_2 . The parameter f_2 determines the masses of the lensing galaxy and the cluster. If the cluster is relatively more massive, then the galaxy is relatively less massive. In this case f_2 is relatively larger. This is important because the lensing galaxy can be

significantly less massive compared with the case where there is no cluster contribution. A best fitting model has $\chi^2 \approx 6.25$ and is obtained when $f_2 \approx 0.0011$, for which $\text{P.A.}_{12} \approx -98^\circ$ (Model 1, Table 5; Fig. 3). As f_2 increases from this value, χ^2 increases only moderately. However, for $f_2 \gtrsim 0.0025$, the total magnification is $\mathcal{M}_{tot} \gtrsim 600$. Thus, $f_2 = 0.0024$ is the upper limit, since we require the total magnification not be larger than 600 (see the introduction of §3). The model with $f_2 = 0.0024$ is given in Table 5 (Model 2). As f_2 decreases from 0.0011, χ^2 increases rapidly. We set the lower limit on f_2 at the 99% confidence level from the best fitting model. The lower limit is $f_2 = 0.0003$ (Model 3, Table 5). For the range of $f_2 = 0.0003$ to 0.0024 the mass of the lensing galaxy inside $0''.6$ (which is approximately the Einstein radius) ranges from $0.78 \times 10^{11} M_\odot$ to $1.84 \times 10^{11} M_\odot$ with the best fitting value of $1.22 \times 10^{11} M_\odot$. Our best fitting model (Model 1) is much more consistent with the observational relative amplifications than is the Kneib et al. (1998a) galaxy+cluster model (their Model 2). This improvement was achieved only when we allowed the parameter P.A._{12} to be a free parameter. The best fitting value of -98° is significantly different from the value of -144° for the Kneib et al. (1998a) model (the cluster center is more westward in our model). This is, of course, not an issue since no reliable determination of the mass center of the possible cluster is known at present. Rather, our study suggests that a cluster (if it is truly present) should be positioned $\sim 46^\circ$ more westward than Kneib et al. (1998a) found.

3.5. BEL/Continuum Ratio and a Size-Scale Constraint on the BEL Region

Finally, we turn to the question of the lower BEL/continuum ratio for component D. Using our lens models (EM+ γ , two-galaxy, and galaxy+cluster models), we have examined the macrolensing interpretation of the lower BEL/continuum ratio for component D. To consider this we studied the magnification of a circular region on the source plane. A lensed image of a circular source will not be circular, but will have a deformed shape, and its angular area will be different from that of the source. We studied how the angular areas of the image components vary as the radius of the source increases. We found that for our lens models, the ratios of the angular areas of the image components changed little up to the point where two of the components merged (components A and B merged first). In particular, the ratio of the angular area of component D to that of component C does not decrease as the radius increases. Even if an elliptical source is considered, it does not make any significant difference. Thus, the lower BEL/continuum ratio for component D cannot be explained by macrolensing using our lens models.

As was noted in the beginning of §3, the most plausible interpretation is that component D is microlensed. Since microlensing amplification depends on the size of the source region, the pointlike continuum region and the more extended BEL region will be amplified differently. While we can be confident that the continuum region is amplified by a small mass, we do not know to what degree the BELR is amplified by the small mass since we do not know the extent of the BELR. Whether or not a source region will be affected by a microlens is determined by the

characteristic length η_0 on the source plane (Schneider, Ehlers, & Falco 1992). For a star of mass M at $z = 1.55$, it is given by

$$\begin{aligned} \eta_0 &\approx 0.0061(M/M_\odot)^{1/2}h_{75}^{-1/2}\text{pc} \\ &\approx 1.9 \times 10^{16}(M/M_\odot)^{1/2}h_{75}^{-1/2}\text{cm}, \end{aligned} \tag{4}$$

where we take $q_0 = \frac{1}{2}$ and $\Lambda = 0$. If the BELR is larger than η_0 , it will not be significantly affected by microlensing. Otherwise, the BELR will be amplified, as will the continuum. In using R_{DC} as a lensing constraint in §3.1 – §3.4, we assumed that the BELR was not amplified by a microlens. However, this assumption was excluded when we considered the two-galaxy lens model with the secondary galaxy at the position of object 14 in §3.3.2. It is therefore interesting that the lens model of §3.3.2 requires that the BELR be amplified. This is important because if the model is correct, and all the other models could be rejected observationally (e.g. the proposed secondary galaxies in §3.3.1 turn out not to exist and the possible cluster in §3.4 does not have a significant lensing effect because it is not sufficiently massive), the BELR must be as large as, or *smaller* than, η_0 . A detailed study of microlens models could then be used to determine or constrain the physical size of the BELR.

The likelihood of microlensing along a light path is determined by the “optical depth” to microlensing, which is given by the ratio of surface mass density of microlensing matter to the critical mass density $\Sigma_{cr} = (4\pi G/c^2)^{-1}(D_d D_{ds}/D_s)^{-1}$ (Paczynski 1986). The two-galaxy models have qualitatively different microlensing probabilities for the image components compared with the EM+ γ model and the galaxy+cluster models. In the two-galaxy lens models (from both §3.3.1 and §3.3.2) component D has the largest microlensing probability, while in the other models component D has a slightly smaller probability than component B and/or C. More specifically, component D has $\approx 6 - 31\%$ higher microlensing probability than component A (or C) which has the second largest microlensing probability in the two-galaxy lens models. Thus, the microlensing interpretation of component D favors the two-galaxy model over the single-galaxy, external-shear model and the galaxy+cluster model.

4. Discussion

We have argued that a single-galaxy model is inconsistent with the HST observations (T97). While the introduction of an external shear to a single galaxy can fit the image positions well, the predicted relative magnifications do not match well the observationally-derived relative amplifications (§3.2). Two possibilities have been considered to explain this. One possibility is that none of the dust extinction models used by T97 to derive the relative amplifications accurately model the true dust extinctions, i.e., the dust extinctions might be more complicated than assumed by T97. Note that T97 had to assume the type and redshift of the dust since they

were not known from observations. Because of this, we were conservative in using the relative amplifications of T97 as lensing constraints; we used 10% as uncertainties. Yet, the single-galaxy, external-shear model is still not very successful in matching the amplifications. Moreover, since the NICMOS-2/F160W intensity ratios (Kneib et al. 1998b) are consistent with the T97 amplification models A, B, and D (Table 2), which are similar to one another, this bolsters our conclusion that a single-galaxy, external-shear model is not an appropriate description of the lens in the Cloverleaf, although the model is relatively simple. In other words, the quadrupole term (eq. [3]) alone may not appropriately account for a secondary lensing contribution.

The other possibility we considered were new lens models of the Cloverleaf. Specifically, we considered lens models consisting of two elliptical masses; two-galaxy models (§3.3) and galaxy+cluster models (§3.4). In the two-galaxy models we considered a secondary galaxy either at an arbitrary position (§3.3.1) or at the position of a detected object (§3.3.2). The two-galaxy models of §3.3.1 can fit the observationally-derived relative amplifications nearly perfectly. The two-galaxy model of §3.3.2 can fit R_{AC} and R_{BC} well, but its predicted R_{DC} is significantly lower than the observed R_{DC} . The galaxy+cluster model does not fit the relative amplifications as well as the two-galaxy models of §3.3.1, but it does fit somewhat better than the single-galaxy, external-shear model. In the two-galaxy models of §3.3.1 the secondary galaxy is much less massive (and thus much fainter, assuming a similar mass-to-light ratio) than the primary galaxy. Given that the primary galaxy is so faint that it has never been detected at optical wavelengths, it may not be a problem that the secondary galaxy has not been detected. Even with future observations it will be a challenge to detect a relatively faint galaxy in the bright region of the Cloverleaf. As our study shows, the position of the secondary galaxy is not uniquely determined, but we proposed three possible regions of sky for the unseen galaxy [see Figure 1 (a), (b), and (c)]. The assumption behind these two-galaxy models is that neither galaxy 14 nor a possible cluster makes a significant contribution to the lensing; in other words, we need an unseen lensing contributor. Along the line-of-sight to the Cloverleaf, absorption systems exist at many different redshifts (Monier et al. 1998), and two galaxies may happen to lie along the line-of-sight. The two galaxies could be at different redshifts independent of each other, or at nearly the same redshift. For example, they could be a binary system of galaxies, or two galaxies in the process of merging. There are at least two other lens systems where it is believed/speculated that the lens may be two galaxies, namely MG2016+112 (Lawrence et al. 1984; Nair & Garrett 1997) and B1608+656 (Myers et al. 1995; see, however, Fassnacht et al. 1996). One possible difficulty with the two-galaxy model at present is that the predicted position of the primary galaxy is not in good agreement with the observed position of the detected light (Kneib et al. 1998b). However, none of the models considered in this paper match the observed galaxy position within the observational uncertainty. The discrepancies could be explained by the misalignments between the light and mass.⁵ The

⁵More radically, the light could be a ghost image arising from the four bright QSO components. This possibility should not be excluded until the properties of HST NICMOS images are better quantified. In this case, a primary galaxy in the two-galaxy model can be near components A & B while a secondary galaxy is near components C & D

galaxy+cluster lens model for the Cloverleaf was first considered by Kneib et al. (1998a) based on the detection of the overdensity of objects in the surrounding of the Cloverleaf. As was shown in our study, if the cluster position is fixed at the position used by Kneib et al. (1998a), the model does not fit the observed relative amplifications very well. However, if we allow the position angle of the cluster mass center (viewed from the lensing galaxy) to be a free parameter, we can improve the fit significantly. The best fitting model predicts that the cluster mass center is positioned roughly west of the Cloverleaf ($\text{P.A.}_{12} \approx -98^\circ$). (In the Kneib et al. 1998a model, the cluster is positioned south-west of the Cloverleaf.) The two-galaxy model with the secondary galaxy’s position constrained (§3.3.2) is more realistic than other models in that an *observed* galaxy is used as the secondary galaxy, while in the other models the secondary lensing contributors are either unconfirmed or hypothetical. However, in order for the model to be consistent with the dust-extinction-corrected relative amplifications, component D must be microlensed. Furthermore, not only the continuum but also the BEL should be amplified by microlensing. This requirement of the model is not discrepant with present observations since microlensing of component D is very likely (§1, §3) and the physical size of the BELR is unknown.

As was shown in §3.5, the microlensing interpretation of component D favors the two-galaxy models over the galaxy+cluster models since component D has the largest microlensing probability in the two-galaxy models, while it does not in the galaxy+cluster models. Kneib et al. (1998a) argued that a cluster is present along the line of sight to the Cloverleaf. However, its mass distribution is not known at present, and thus we do not know how much of a lensing effect it will have on the Cloverleaf. Future observational studies (e.g. using AXAF) of any cluster will be useful for studying its lensing effect.

A long-period (1987-1994) monitoring program of the Cloverleaf by Østensen et al. (1997) did not result in the detection of time delays between image components. However, upper limits of 150 days (99% confidence) were put on the time delays. This is consistent with our lens models. Measurements of time delays from future monitoring of the Cloverleaf will be useful to distinguish between models. Two-galaxy models predict that component C is the leading image, followed by components B, A, and D, which is the trailing image. The maximum time delay between the leading and trailing images ranges between $\approx 20 - 40$ days. In the galaxy+cluster lens models component A may lead component B; however, components C and D are still the leading and trailing images. The maximum time delay is $\approx 7 - 13$ days.

More work will have to be done to determine if the Cloverleaf is a good candidate for determining the Hubble constant. To determine the Hubble constant, time delays between the image components must be measured and the mass distribution of the lens must be well-determined, consistent with observational constraints. At present, neither of these conditions has been met for the Cloverleaf. As our study shows, time delays in the Cloverleaf are likely to

as opposed to Model 1 [Fig. 1 (a)].

be neither too short nor too large to raise observational difficulties.⁶ For the determination of the mass distribution of the lens, it should be a priority to spectroscopically identify the reported lensing galaxy and observe its properties in detail. It will also be useful to observationally study “galaxy 14” and the possible cluster. Another important observational task is to revisit the relative amplification models of T97 in order to determine the macrolensing magnification ratios more reliably and accurately. This could be done with better infrared data. With observational knowledge of the lens and better data on the lensing properties in the future, the mass distribution of the lens could be well-determined.

We thank Valery Khersonsky for discussions on mass models of lenses in the early stages of this work and Cyril Hazard for reading the early draft of the manuscript and commenting on it. We also thank Jean-Paul Kneib for valuable comments and suggestions for the improvement of the manuscript. K. H. C. acknowledges partial support from the Zaccheus Daniel predoctoral fellowship at the University of Pittsburgh during some phase of this work.

REFERENCES

- Angonin, M.-C., Remy, M., Surdej, J., & Vanderriest, C. 1990, *A&A*, 233, L5
- Buote D.A., & Canizares, C.R. 1996, *ApJ*, 457, 565
- Chae, K.-H., Khersonsky, V.K., & Turnshek, D.A. 1998, *ApJ*, 506, 80 (CKT)
- de Theije, P.A.M., Katgert, P., & van Kampen, E. 1995, *MNRAS*, 273, 30
- Falco, E., et al. 1998, private communication
- Fassnacht, C.D., Womble, D.S., Neugebauer, G., Browne, I.W.A., Readhead, A.C.S., Matthews, K., & Pearson, T.J. 1996, *ApJ*, 460, L103
- Fischer, P., Bernstein, G., Rhee, G., & Tyson, J.A. 1997, *AJ*, 113, 521
- Hazard, C., Morton, D.C., Terlevich, R., & McMahon, R. 1984, *ApJ*, 282, 33
- Hutsemékers, D. 1993, *A&A*, 280, 435
- Hutsemékers, D., Surdej, J., & Van Drom, E. 1994, *Astrophysics and Space Science*, 216, 361
- Kayser, R., Surdej, J., Condon, J.J., Kellermann, K.I., Magain, P., Remy, M., & Smette, A. 1990, *ApJ*, 364, 15
- Keeton, C.R., & Kochanek, C.S. 1997, *ApJ*, 487, 42
- Keeton, C.R., Kochanek, C.S., & Seljak, U. 1997, *ApJ*, 482, 604 (KKS)
- Kneib, J.-P., Alloin, D., Mellier, Y., Guilloateau, S., Barvainis, R., & Antonucci, R. 1998a, *A&A*, 329, 827

⁶See, however, Yun et al. (1997) who predicted very short time delays of ~ 1 day.

- Kneib, J.-P., Alloin, D., & Pelló, R. 1998b, *A&AL*, preprint (astro-ph/9804207)
- Kovner, I. 1987, *ApJ*, 312, 22
- Lawrence, C.R., et al. 1984, *Science*, 223, 46
- Lewis, G.F., & Belle, K.E. 1997, *MNRAS*, preprint (astro-ph/9711017)
- Magain, P., Surdej, J., Swings, J.-P., Borgeest, U., & Kayser, R. 1988, *Nature*, 334, 325
- Monier, E.M., Turnshek, D.A., & Lupie, O.L. 1998, *ApJ*, 496, 177
- Myers, S.T., et al. 1995, *ApJ*, 447, L5
- Nair, S., & Garrett, M.A. 1997, *MNRAS*, 284, 58
- Østensen, R., et al. 1997, *A&A Supplement*, 126, 393
- Paczyński, B. 1986, *ApJ*, 304, 1
- Press, W.H., Teukolsky, S.A., Vetterling, W.T., & Flannery, B.P. 1992, *Numerical Recipes* (2nd ed.; Cambridge: Cambridge Univ. Press)
- Remy, M., Gosset, E., Hutsemékers, D., Revenaz, B., & Surdej, J. 1996, in *Astrophysical Applications of Gravitational Lensing, Proceeding of the 173 Symposium of the International Astronomical Union*, eds. C. Kochanek and J. Hewitt, Kluwer, 261
- Schneider, P., Ehlers, J., & Falco, E.E. 1992, *Gravitational Lenses* (New York: Springer-Verlag)
- Turnshek, D.A., Lupie, O.L., Rao, S.M., Espey, B.R., & Sirola, C.J. 1997, *ApJ*, 485, 100 (T97)
- Yun, M.S., Scoville, N.Z., Carrasco, J.J., & Blandford R.D. 1997, *ApJ*, 479, L9

Table 1
HST Astrometric Data

Component	Δ RA (err) (arcsec)	Δ Dec (err) (arcsec)
Comp A	0.000	0.000
Comp B	0.744 (0.003)	0.172 (0.003)
Comp C	-0.491 (0.003)	0.716 (0.004)
Comp D	0.355 (0.003)	1.043 (0.012)
G1 ¹	0.12 (0.040)	0.50 (0.040)

¹ This position of the primary galaxy is from the analysis of HST NICMOS-2 data (Kneib et al. 1998b).

Table 2
“Dust-Extinction-Corrected” Relative Amplifications based on HST photometry

Relative Amplifications ⁵	Model A ¹	Model B ²	Model C ³	Model D ⁴
R_{AC}	1.65	1.68	2.21	1.63
R_{BC}	1.62	1.61	2.31	1.55
R_{DC}^6	0.95	0.95	1.01	0.95

¹ Results assuming Galactic Extinction at $z = 2.55$

² Results assuming SMC Extinction at $z = 2.55$

³ Results assuming Galactic Extinction at $z = 1.55$

⁴ Results assuming SMC Extinction at $z = 1.55$

⁵ The adopted uncertainties we use in the lens models are 10% of these values.

⁶ This represents the amplification before the possible microlensing amplification is corrected (see §3). To correct for the microlensing amplification of the continuum, this ratio should be multiplied by 0.7.

Table 3
Single-Galaxy Lens Models

	EM Model	EM+ γ Model
χ^2	168.3	12.76
N_{dof}	4	4
Σ_0 ($M_\odot \text{ pc}^{-2}$)	2.95×10^4	1.13×10^7
ν	1.19	2.00 (fixed)
r_c ($h_{75}^{-1} \text{ kpc}$)	0.001	0.001 (fixed)
ϵ	0.059	0.425
P.A. ($^\circ$)	22.0	140.3
γ	—	0.217
θ_γ ($^\circ$)	—	43.6
Predictions		
\mathcal{M}_{tot}	373	36.3
R_{AC}	1.15	1.56
R_{BC}	1.16	1.35
R_{DC}	0.85	0.84
τ_{AC} ($h_{75}^{-1} \text{ days}$)	3.93	7.38
τ_{BC} ($h_{75}^{-1} \text{ days}$)	1.28	2.61
τ_{DC} ($h_{75}^{-1} \text{ days}$)	6.36	15.9
\vec{x}_{AG1} ($''$, $''$)	(0.165, 0.515)	(0.157, 0.547)

Table 4
Two-Galaxy Lens Models

	Model 1	Model 2	Model 3	Model 4 ^{1,2}
χ^2	5.43	7.61	7.69	6.39
N_{dof}	2	2	2	2
Σ_0^{tot} ($M_\odot \text{ pc}^{-2}$)	1.204×10^7	1.298×10^7	1.417×10^7	1.617×10^7
f_2	0.174	0.211	0.260	0.351
ϵ_1	0.340	0.340	0.355	0.172
P.A. ₁ ($^\circ$)	23.6	49.6	0.5	124.2
ϵ_2	0.540	0.796	0.572	0.84
P.A. ₂ ($^\circ$)	36.9	-6.9	43.1	31.5
d_{12} ($''$)	0.5 (fixed)	1.3 (fixed)	1.6 (fixed)	3.96
P.A. ₁₂ ($^\circ$)	130.0	-4.5	-129.5	24.7
\vec{x}_{G1S} ($''$, $''$)	(0.050, -0.076)	(-0.026, 0.090)	(-0.167, -0.128)	(0.022, 0.284)
Predictions				
\mathcal{M}_{tot}	22.6	17.9	17.0	41.8
R_{AC}	1.64	1.68	1.63	1.78
R_{BC}	1.60	1.59	1.62	1.58
R_{DC}	0.70	0.66	0.68	0.43
τ_{AC} (h_{75}^{-1} days)	15.9	17.8	19.7	6.9
τ_{BC} (h_{75}^{-1} days)	8.6	9.4	8.7	3.5
τ_{DC} (h_{75}^{-1} days)	25.7	40.8	36.1	21.9
\vec{x}_{AG1} ($''$, $''$)	(0.105, 0.590)	(0.216, 0.553)	(0.214, 0.557)	(0.205, 0.544)

¹ In this model the position of G2 is constrained by the observed position of object 14 (see §3.3.2).

² In this model R_{DC} was not used in the calculation of χ^2 .

Table 5
Galaxy+Cluster Lens Models

	Model 1	Model 2	Model 3
χ^2	6.25	10.66	16.18
N_{dof}	3	3	3
$\Sigma_0^{tot} (M_\odot \text{ pc}^{-2})$	5.52×10^6	3.53×10^6	8.38×10^6
f_2	0.0011	0.0024	0.0003
$r_c^{(1)} (h_{75}^{-1} \text{ kpc})$	0.001 (fixed)	0.001 (fixed)	0.001 (fixed)
ϵ_1	0.360	0.333	0.305
P.A. _{.1} (°)	135.7	132.6	139.4
$r_c^{(2)} (h_{75}^{-1} \text{ kpc})$	40 (fixed)	40 (fixed)	40 (fixed)
ϵ_2	0.5 (fixed)	0.5 (fixed)	0.5 (fixed)
P.A. _{.2} (°)	17.2	26.3	35.3
$d_{12} (")$	8 (fixed)	8 (fixed)	8 (fixed)
P.A. _{.12} (°)	-98.2	-68.8	-135.1
$\vec{x}_{G1S} (", ")$	(-6.621, 0.345)	(-8.892, 3.876)	(-1.421, -1.058)
Predictions			
\mathcal{M}_{tot}	185.2	583.4	60.6
R_{AC}	1.52	1.44	1.28
R_{BC}	1.67	1.67	1.32
R_{DC}	0.76	0.58	0.84
$\tau_{AC} (h_{75}^{-1} \text{ days})$	2.96	4.86	7.07
$\tau_{BC} (h_{75}^{-1} \text{ days})$	4.11	6.80	3.68
$\tau_{DC} (h_{75}^{-1} \text{ days})$	11.2	6.74	13.0
$\vec{x}_{AG1} (", ")$	(0.193, 0.535)	(0.220, 0.519)	(0.171, 0.548)

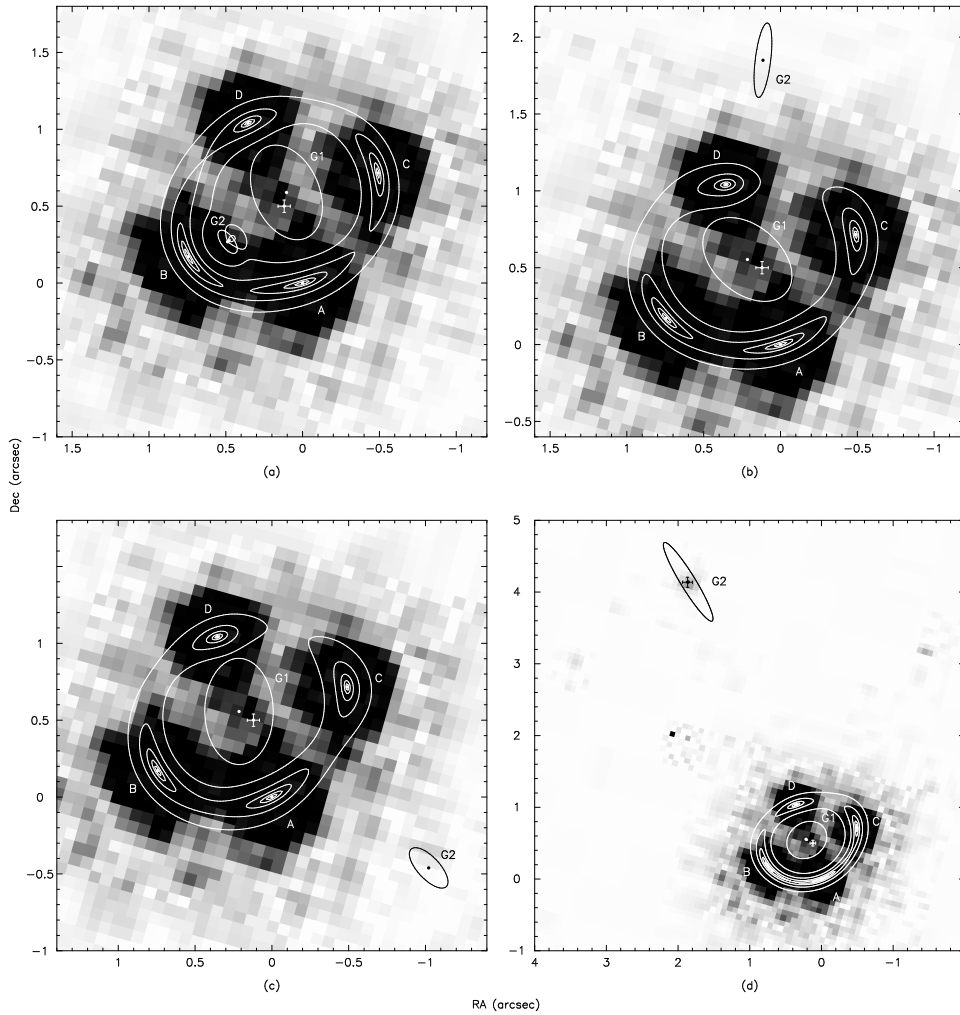


Fig. 1.— Image configuration of two-galaxy lens models (Table 4). The model image is overlaid on the HST NICMOS/F160W image. The five contour levels correspond to 40, 80, 160, 320, and 640 pc from the center of the QSO on the source plane. In the NICMOS image, light (probably from the primary lensing galaxy) is clearly present near the geometrical center of the Cloverleaf. The ellipses representing the galaxies correspond to a surface density of unity convergence ($\kappa = 1$). The observed positions of the QSO components and the primary galaxy are represented by dots with error bars (note that the error bars for the QSO components are too small to be visible). The mass centers of the model galaxies are also represented by dots. North is on the top and east is to the left. (a) Model 1: The secondary galaxy (G2) is positioned southeast of the primary galaxy (G1). (b) Model 2: G2 is positioned north of G1. (c) Model 3: G2 is positioned southwest of G1. (d) Model 4: In this model a detected galaxy (object 14; Kneib et al. 1998a,b) is used as the secondary galaxy. The observed position of the secondary galaxy is represented by a dot with error bars.

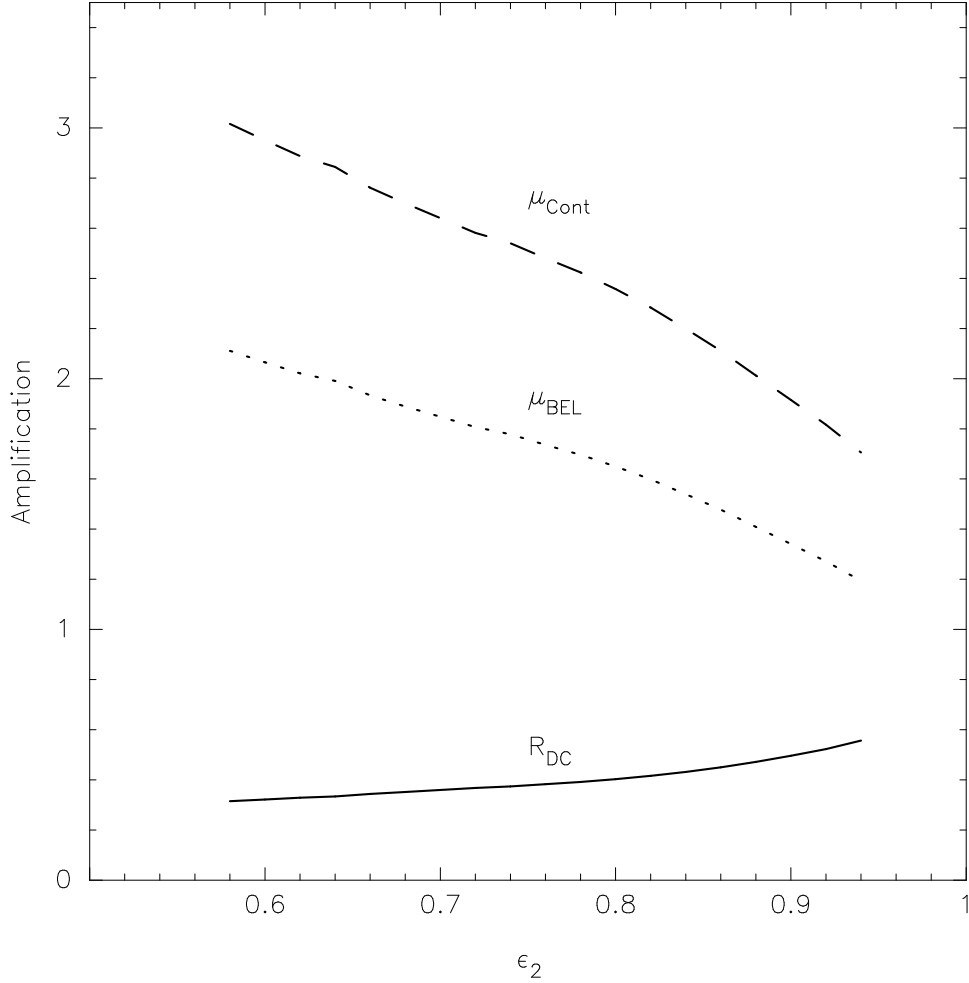


Fig. 2.— Predicted relative magnification of component D (R_{DC}) and the required microlensing magnification factors of the continuum and the BELR as a function of ϵ_2 (G2’s ellipticity) in the two-galaxy lens model of §3.3.2. The model requires that the BELR as well as the continuum be amplified (with the continuum being more amplified) by microlensing in order to be consistent with the dust-extinction-corrected relative amplification of T97 (see §3.3.2). A model with a smaller ϵ_2 predicts a larger microlensing amplification.

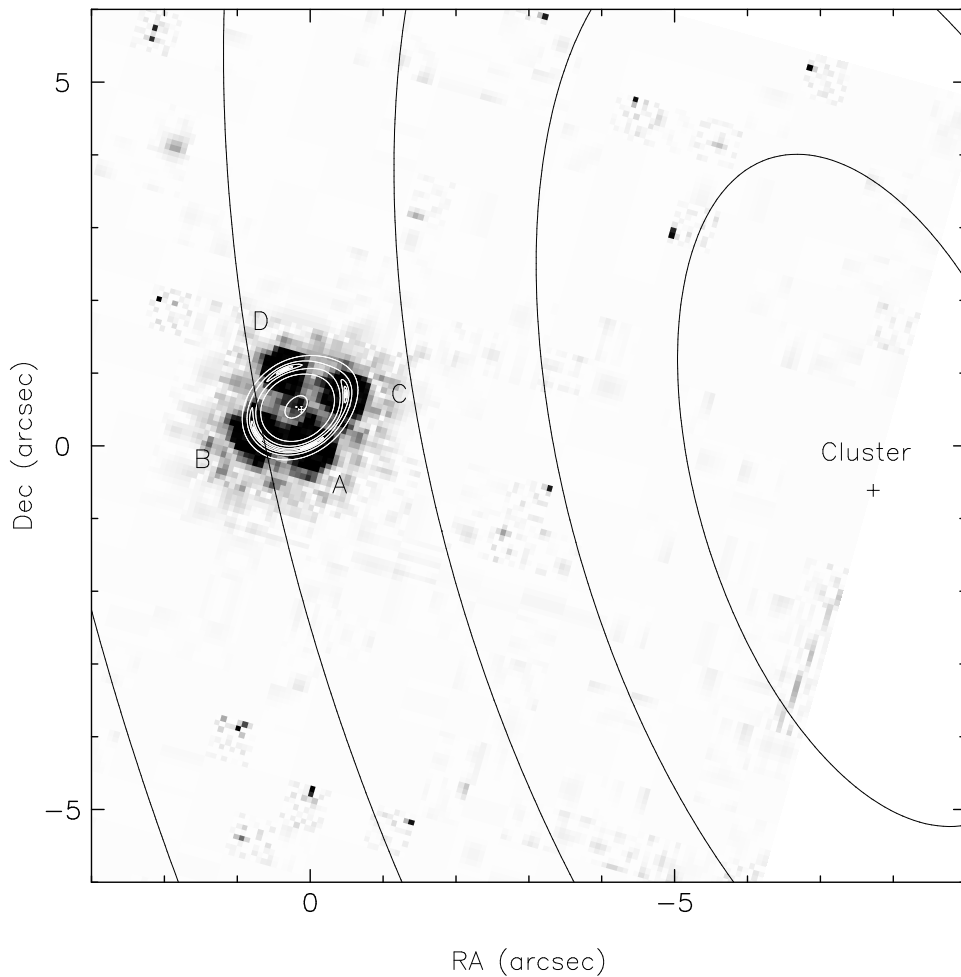


Fig. 3.— Galaxy+Cluster Model 1 (Table 5). The cluster’s mass center is at $8''$ (fixed) west of the lensing galaxy. The contours of the cluster mass distribution correspond to convergence $\kappa = 0.4, 0.5, 0.6, 0.7,$ and 0.8 from east to west. The five contour levels of the image correspond to 20, 40, 80, 160, and 320 pc from the center of the QSO on the source plane. North is on the top and east is to the left.